A Dual Layer Hair Array of the Brown Lacewing: Repelling Water at Different Length Scales

Jolanta A. Watson,[†*] Bronwen W. Cribb,[‡] Hsuan-Ming Hu,[†] and Gregory S. Watson[†]
[†]School of Pharmacy and Molecular Sciences, James Cook University, Townsville, Queensland, Australia;
and [‡]Centre for Microscopy & Microanalysis and School of Biological Sciences, The University of Queensland, St. Lucia, Queensland, Australia

ABSTRACT Additional weight due to contamination (water and/or contaminating particles) can potentially have a detrimental effect on the flight capabilities of large winged insects such as butterflies and dragonflies. Insects where the wing surface area-body mass ratio is very high will be even more susceptible to these effects. Water droplets tend to move spontaneously off the wing surface of these insects. In the case of the brown lacewing, the drops effectively encounter a dual bed of hair springs with a topographical structure which aids in the hairs resisting penetration into water bodies. In this article, we demonstrate experimentally how this protective defense system employed by the brown lacewing (*Micromus tasmaniae*) aids in resisting contamination from water and how the micro- and nanostructures found on these hairs are responsible for quickly shedding water from the wing which demonstrates an active liquid-repelling surface.

INTRODUCTION

Insects demonstrate a remarkable diversity in the way they contend with the elements of nature. For many insects, the environmental conditions are harsh and their ability to maintain adequate mobility is vital for survival. How insects interact with water bodies of various sizes is an important aspect, inasmuch as it is seldom possible to escape contact. The water contact angles of insect surfaces show a wide range of variation which is broadly correlated with surface roughness and with habitat. Holdgate (1) has characterized four major groups of insects in relation to their water wetting properties. Among the most interesting groups are the terrestrial and aquatic species, whose surfaces are very rough or covered with hair piles. They have very high advancing and receding contact angles, often $>150^{\circ}$. Generally, insects which have a very high wing surface area/body mass ratio (SA/M), and/or throughout their life cycle come into contact with water sources, typically have these adaptations. These adaptations are more often than not structural rather than chemical, because insect cuticle surfaces are made up of a chemistry that is at the near upper limit of hydrophobicity for smooth surfaces (1).

The structural differences which reflect how numerous insects have solved a common problem by achieving antiwetting surfaces are quite remarkable. Many butterflies and moths possess scales with a typical overlaying tile type arrangement. These scales exhibit micron and submicron structure in the form of longitudinal and lateral ridges (2). One study (3) examining 29 species of butterflies attributed the superhydrophobic nature of the wings to the micro and submicroscale structuring. A number of other functional properties have also been attributed to scales on butterflies including camouflage display, signaling, and possibly thermoregulation control (3–5). As well, scales can detach as an aid for protection against highly adhesive surfaces (e.g., spider webs) (6).

In contrast, the dragonfly and planthopper present surface topographies with rodlike structures (papilla) forming a layer of structured matting. These structures are typically several hundred nanometers in height and <100 nm in width and between 100 and 200 nm in spacing with a high numerical structure density of 40–80 per square micrometer (7). Similar structures have also been found on damselflies (8). In that study, the authors suggested a number of possible functions for the waxlike covering. In addition to offering protection against water, the authors proposed that the structuring may aid in intra/interspecific communication based on ultraviolet light reflection of the layer.

The multiple functions that micro/nanostructuring can serve on insect surfaces (especially wings) is demonstrated on numerous insects. For example, antiwetting structures on a number of cicada species exhibit dimensional profiles from nanometers to several microns; generally spherically capped conical protuberances (9,10). Structures in the smaller size range with a spacing and height of ~200 nm and a radius of curvature of 35–55 nm have been shown to be functionally effective as an antireflective surface which presumably helps to camouflage the insect from predators (9). These surfaces also demonstrated low adhesion with hydrophilic particles (9).

There are a number of theories that express the antiwetting nature and superhydrophobic properties of insect surfaces, all of which have intrinsic assumptions and limitations (11–15). Cassie and Baxter (11) represent the superhydrophobic state in terms of a number of interfaces, a liquid-air interface with the ambient environment surrounding the droplet and a surface under the droplet involving solid-air, solid-liquid, and liquid-air interfaces.

Submitted September 6, 2010, and accepted for publication December 20, 2010.

*Correspondence: jolanta.watson@jcu.edu.au

Editor: Levi A. Gheber.

0006-3495/11/02/1149/7 $2.00

doi: 10.1016/j.bpj.2010.12.3736

Equation 1 shows the contact angle formed with a rough surface,

$$\cos\theta_C = R_f f_{SL}\cos\theta + f_{SL} - 1, \quad (1)$$

where R_f is the roughness factor defined by the ratio of the true solid/liquid area to its projection on a flat plane (the roughness factor of the wetted area) and f_{SL} is the fraction of the solid/water interface (the area fraction of the projected wet area), and θ represents the contact angle which would occur on a smooth surface with the identical chemistry and can be expressed by the Young's relation

$$\theta = \cos^{-1}[(\gamma_{SV} - \gamma_{SL})/\gamma_{LV}],$$

where the γ_{ij} terms correspond to the solid-vapor, solid-liquid, and liquid-vapor interfacial energies/tensions, respectively. Equation 1 necessitates the surface to have the required roughness to trap air in topographically favored regions such as troughs and surface depressions. The insect species described above demonstrate this common theme in that their specialized yet diverse topographies minimize the solid-liquid contact area and maximize the liquid-air contact.

The Planipennia is one of the oldest forms of endopterygote Neoptera. The adult can range in size from very large insects with wing spans in excess of 150 mm to quite small species with wing spans of ~5 mm. Most lacewing species fly rather slowly and irregularly and in these cases the wing-coupling mechanism, if present, appears inefficient. Many species are cryptically colored and many are dressed with long hairs. As with other insect cuticular structures, hairs may serve multifunctional purposes such as aiding in flight (contributing to aerodynamic factors), reducing contact with solids and protection against wetting. The brown lacewing in this study (*Micromus tasmaniae*) is a small insect with a very high wing SA/M ratio and thus is susceptible to detrimental adhesional contacts. In the worst-case scenario, the insect could become a victim of permanent immobilization on water or wetted surfaces with a reduced capacity to evade or fight off predators. We demonstrate how the brown lacewing uses a dual layer array of hair springs to repel water and how the microstructure aids in this function. We also show differences between this lacewing and other lacewing species which do not have a dual protection of hairs to resist water contamination.

MATERIALS AND METHODS

Insect preparation

The brown lacewings (*Micromus tasmaniae*) were caught in the local areas of outer Brisbane, Australia. Wing samples (forewings) were excised from six lacewing insect bodies using a sterile scalpel. Experiments were conducted on the lacewing within 48 h of capture at room temperature (20–25°C).

Photographic imaging

Photographs shown in Fig. 1, *A* and *B*, were obtained using a Digital 350D SLR, and Ultrasonic EF-S 60 mm macro lens at an 80 megapixel resolution (both by Canon Australia, North Ryde, New South Wales, Australia).

Optical microscopy

Optical imaging shown in Fig. 1 *C* and Fig. S3 in the Supporting Material were obtained using an AIS Optical Microscope VG8 (Australian Instrument Services, Croydon, Victoria, Australia) coupled with a color closed-circuit television camera WV-CP410/G (Panasonic, Osaka, Japan) attached, which allowed image capture at 40× magnification.

Optical image shown later in Fig. 3 was acquired with an OPTEM 100C Series 10:1 Zoom Optical System (Thales, Neuilly-sur-Seine, France) fitted with a 40×/0.60 objective and 10-mm fiber optic adaptor (Carl Zeiss, Oberkochen, Germany). The source of incident light was a 150-W lamp

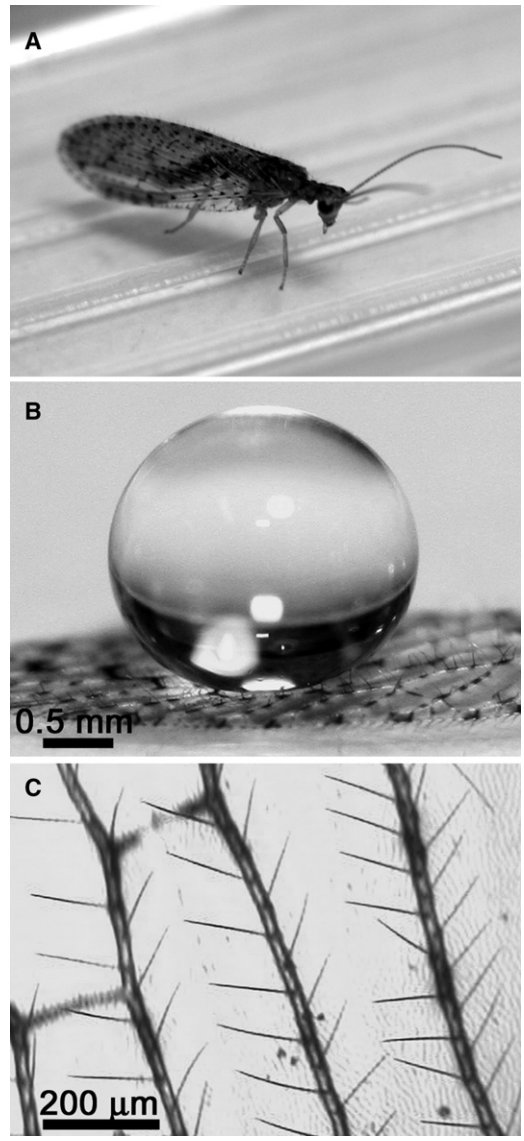

FIGURE 1 Optical images of the brown lacewing *Micromus tasmaniae* (*A*), a water droplet on the wing demonstrating an apparent contact angle of 180° (*B*), and the macrotrichia (large hair) arrangement on the wing veins (*C*).

(ellipsoidal dichroic reflector, or EKE-type) with transmission from 400 to 700 nm.

Scanning electron microscopy

In the case of scanning electron microscope (SEM) imaging (Fig. 2 and later in Fig. 6, and Fig. S1, Fig. S2, and Fig. S4), individual hairs attached to atomic force microscopy (AFM) probes were placed on an aluminum pin-type stub with carbon-impregnated double-sided adhesive, then sputter-coated with 7–10 nm of platinum, before being imaged using a 6300 field emission (JEOL, Tokyo, Japan) SEM at 8 kV. Wing tissues of the lacewing (~3 mm × 3 mm) were excised and imaged under the same conditions.

Atomic force microscopy

A TopoMetrix Explorer TMX-2000 SPM (Veeco Instruments, Plainview, NY) was used to obtain atomic force microscopy (AFM) measurements including hair mechanical properties and adhesion data. This was carried out in the Force-versus-distance (F-d) mode (16). A 130 × 130 μm^2 tripod scanner was used with a z range of 9.7 μm. F-d curves were acquired at rates of translation in the z direction in the range 2–5 $\mu m\ s^{-1}$, with each curve consisting of 600 data points. The analyses were carried out under air-ambient conditions (temperature of 20–25°C and 60–75% relative humidity). Beam-shaped tipless levers (Ultrasharp; NT-MDT, Tallinn, Estonia) were used for the attachment of hairs and also determination of hair spring constants. Calibration along the z direction and the force constants of levers (k_N) were determined by methods described in the literature (17,18).

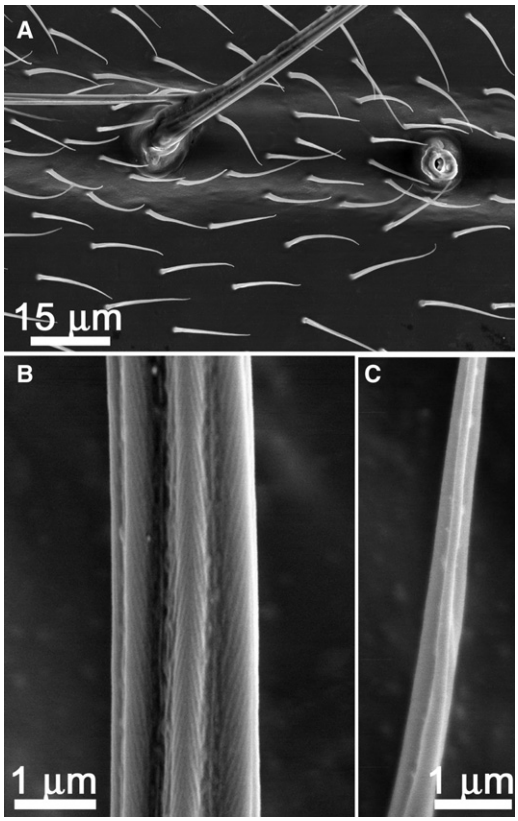

FIGURE 2 Scanning electron microscope images revealing (*A*) a dual layer of hairs on the wing of *Micromus tasmaniae*, (*B*) showing the fine, open-sheeted ridge structure found on the *Micromus tasmaniae* macrotrichia, and (*C*) channels running along the long axis of the shaft of the underlying microtrichia.

The force constants of individual lacewing hairs were determined by deflection with a lever of a known spring constant. A quantity of 10–20 F-d curves were obtained on two individual hairs utilizing two tipless beam-shaped levers with similar spring constants (k_N values of 0.1 ± 0.02 N m^{-1}). The measurements were firstly obtained on the uncoated hair. The same hair was then thinly coated with polydimethylsiloxane (PDMS), as described in the section below, and F-d measurements obtained. Later a thick layer of PDMS was applied to the hairs whereby the final F-d measurements were obtained. The adhesional data was obtained by depositing a 10 μL droplet of Milli-Q water (Millipore, Billerica, MA) on a slide previously coated with PDMS to ensure a hydrophobic surface. An uncoated lacewing hair (attached to a lever as described in the section below) was then brought into contact with the droplet (always located ~500 μm below the top of the drop in order to avoid the meniscus attraction between the hydrophilic lever and the Milli-Q water droplet) and retracted with 10–20 F-d curves obtained. The same hair was then coated in a thin layer of PDMS and finally with a thick layer.

Hair attachment and coating

Individual lacewing hairs were scraped off the wing membrane onto clean silicon wafer pieces, using a surgical scalpel. These were then placed under an optical microscope. Tipless levers were attached to an in-house positioning translator fixed to an optical microscope which allowed for precise x, y, and z positioning of the lever. The very end of the lever was firstly lowered onto the edge of a glue droplet (fast curing two-part epoxy resin) coating the underside, and then retracted. The lever was then positioned above an individual lacewing hair aligned with the lever, lowered onto the end of the desired hair, and raised with the hair attached to the end of the lever. The samples were then allowed to dry for 24 h before further experimentation.

Once the initial measurements were obtained, a mixture of 10:1 base/curing agent of PDMS (Sylgard-184; Dow Corning, Midland, MI) was prepared for a thin coating on the hairs. A drop of PDMS was deposited onto a concave microscope slide where the polymer was allowed to spread (~1 min). The slide was then placed under an optical microscope, where a lever with a lacewing hair attached at the free end was then positioned at the edge of the PDMS droplet and gently lowered ensuring full coverage of the hair, but not the lever itself. The hair was retracted and allowed to cure for a minimum of 48 h under ambient conditions before any further experimentation. For a thick coating of PDMS on the hairs, the PDMS mixture placed on the microscope slide was partially cured in the oven for 3 min at 60°C, and then removed and allowed to cool to room temperature. The sample was then placed under the microscope and the hair dipped ~5 times in succession and cured as described above. A similar attachment and coating procedure was applied to measure the spring constants of individual lacewing hairs, but with two individual hairs attached to AFM chips to ensure that one end of the hairs remained fixed.

RESULTS AND DISCUSSION

Fig. 1 *A* shows an optical image of the brown lacewing (*Micromus tasmaniae*). The forewings are ~5 mm in length. The wing membrane interacting with a 10 μL droplet of water exhibits an apparent contact angle with the underlying membrane close to 180° (see Fig. 1 *B*). The hairs (macrotrichia) attached to the veins spaced equidistance apart are visible in the photograph in Fig. 1 *B* and from the optical microscope image in Fig. 1 *C*. Scanning electron microscopy (SEM) images of the brown-lacewing wing shows that there is actually a dual layer of hairs: the larger hairs

(macrotrichia) originating from sockets on the vein regions and smaller hairs (microtrichia) scattered on the wing surface at roughly equal distances apart (~13 μm) (Fig. 2 *A*).

The fine structure of a brown lacewing macrotrichia is shown in Fig. 2 *B*. The hair has a micro/nanoarchitecture consisting of open-sheeted ridges resulting in a number of troughs running along the hair shaft. An SEM cross section of a macrotrichia taken near the midpoint of the hair length on the lacewing is shown in Fig. S1 *A*. At this location the channels show a depth of ~300 nm and radius of curvature of the peaks ~95–130 nm. The microtrichia (smaller hairs) also exhibited micro/nanoarchitecture in the form of channels running along the long axis of the shafts (Fig. 2 *C* and Fig. S1 *B*). The underlying membrane is devoid of structuring (see Fig. S1 *C*). The dimensional parameters of the two hair sizes (macrotrichia and microtrichia) are listed in Table 1.

To investigate whether the fine architecture of the hairs (i.e., the channels) aided in a hair's ability to resist water penetration, individual brown lacewing macrotrichia were coated with PDMS, a hydrophobic polymer, to control the topographical contribution to the process. In the first instance macrotrichia had a thin coat of PDMS applied. Fig. S2 *A* shows an SEM image of an uncoated macrotrichia. Fig. S2 *B* shows that after one thin polymer coat, the nanochannel structure is reduced but still prominent. A subsequent thicker coating removed nanoscale topographical roughness with little trace of the original topography or evidence of channel structures remaining (Fig. S2 *C*).

The interaction of individual hairs (uncoated and coated) with water droplets is shown in Fig. S3. Individual hairs were attached to AFM cantilevers and pressed against the water surface. Neither uncoated nor coated hairs penetrated pure water droplets at force loadings up to 2 μN (Fig. S3, *A* and *B*) so the surface tension of the liquid was modified by addition of sodium-dodecyl sulfate. The thin coated hairs penetrated the surfactant solutions at the same concentration as the uncoated hairs (0.1 M). Thick coated hairs, which resembled a smooth tapered cylinder, were also tested; these penetrated the solution at much lower concentrations of sodium-dodecyl sulfate (0.001 M) (Fig. S3 *C*).

AFM adhesion measurements were carried out on uncoated and coated hairs with water. The AFM is ideally suited for measurements of capillary forces at the micro/nanoscale and adhesion in aqueous and air environments (19). The results showed that uncoated and thin-coated hairs yielded similar adhesion values (42 $\pm$ 9 and 60 $\pm$ 19 nN, respectively) while thick-coated hairs with no residual channel topography exhibited much higher adhesion (>1 μN).

TABLE 1 Macrotrichia and Microtrichia dimensional parameters for the brown lacewing, *Micromus tasmaniae*

Hair type	Diameter at base (μm)	Spacing between hair bases (μm)	Hair length (μm)	Midsection channel depth (μm)
Macrotrichia	4.4 $\pm$ 1.4	32.4 $\pm$ 5.3	144.2 $\pm$ 10.6	0.38 $\pm$ 0.06
Microtrichia	0.7 $\pm$ 0.08	5.8 $\pm$ 1.4	10.7 $\pm$ 1.3	0.16 $\pm$ 0.02

When micron-sized droplets were sprayed onto the lacewing wings, some droplets were supported, or adhered to, the larger hair fibers. This typically resulted in the temporary fixation of droplets above the membrane surface. If unperturbed, these smaller droplets evaporate at the point of contact. Other microdroplets did not come into contact with the underlying wing membrane but were instead supported by the smaller array of hairs fibers as demonstrated in the top and side views in Fig. 3, *A* and *B*, respectively.

Observations under an optical microscope showed that micro droplets are removed from the wing surface by at least three mechanisms:

1. The droplets are mobilized by minor vibrations (e.g., kinetic energy of microdroplets colliding and/or coalescence forces, also observed on carbon nanotubes deposited on silicon micropillars (20), and movements of the wings facilitated by minimal adhesion with the hairs).
2. Larger unstable droplets coming into contact with the hairs absorb microdroplets resting on the smaller hair array.
3. Constant wetting allows microdroplets to build-up in size (hundreds of microns) and are then large enough to roll off the wing surface.

The placement of a stable droplet as seen in Fig. 1 *B* by micropipette was difficult and atypical. The droplets generally rolled off the wing surface unless the wing membrane/cuticle was damaged (e.g., a small segment of the membrane

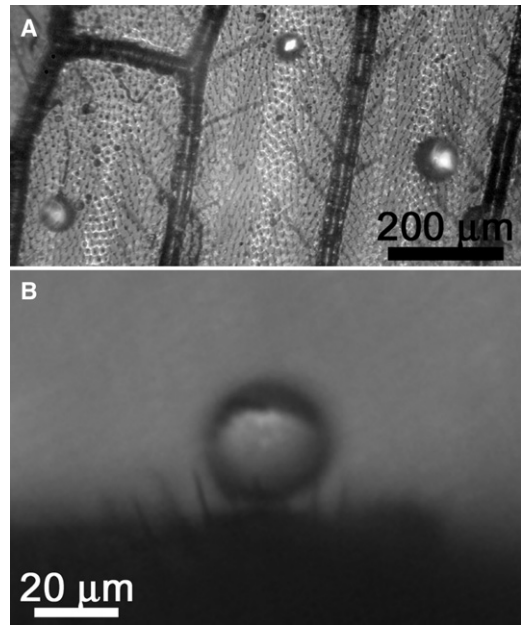

FIGURE 3 (*A*) Top and (*B*) side view optical microscope images showing microdroplets on a *Micromus tasmaniae* wing. The droplets maintain their spherical shape and occupy regions between the macrotrichia arrays, that is, on the microtrichia.

was missing). The droplet seen in Fig. 1 *B* is actually elevated above the wing membrane by >100 μm. The apparent levitation above the surface of the membrane can be explained in relation to the hair arrays on the wing surface. There are several mechanisms whereby hairs can support a droplet above the surface. A study of hairs on a plant leaf (21) showed unexpectedly that the hairs were hydrophilic. In order to understand why a collection of hydrophilic hairs could behave as effectively hydrophobic, the authors considered the hairs as bundles stuck into a liquid-air interface (as shown in the schematic in Fig. 4 *A*) and take into account the elasticity of the hairs. The liquid surface deforms around the hair according to Young's equation (assuming the hairs have a contact angle different from 90°). The surface energy of a liquid is given by

$$f\left(1+|\Delta f^2|\right)^{1/2},$$

where $f(r)$ describes the vertical surface position (21). The cost in terms of energy from deformations of the liquid surface results in attractive forces between the hairs. Thus a number of hairs will group to individual bundles, such that the hairs meet each other at the water-air interface. The tight grouping of hairs will require bending deformation modes which will costs elastic energy. The hairs will bend more strongly if they are moved closer to the substrate, on which the hairs are anchored resulting in a repulsive interaction between the cuticle and the water/air interface. A requirement for the above condition is that the density of hairs is high enough to form a group.

An alternative to the mechanism of hydrophilic interactions that levitate the water droplets above a surface is the case where the hairs are hydrophobic. In this case, they may not penetrate the surface and may act as a series of springs with a restoring force balancing the weight of the droplet (Fig. 4 *B*). The density of hairs on the membrane and the cumulative effect of each hair element will determine the elevation of the droplet above the cuticle. For very small deflections, the force of the droplet (F_{Drop}) would be

$$F_{Drop} = \sum k_N \Delta z, \tag{2}$$

where k_N is the effective individual spring constant and Δz the deflection of the hair.

Optical microscope imaging through the water droplet (from directly above) showed that hairs do not penetrate the surface of the droplet. Thus, the water droplet is supported by the array of micro hairs, resulting in the elevation of the droplet above the wing's surface membrane.

The results from interacting individually coated and uncoated hairs with droplets sheds light on the importance of the micro/nanostructuring in repelling water from the wing surface (Fig. S3). One of the most hydrophobic naturally occurring cuticle surfaces is the wax on the water strider leg ~105° (22). Based on chemistry alone, PDMS-coated hairs represent the upper limit of what can be achieved in nature, inasmuch as the polymer has a measured contact angle with water of ~105° (23). Thinly coated hairs still retained a significant amount of the topographical structure (channels) as seen in Fig. S2 *B*. These, like the uncoated hairs, did not penetrate the 0.1 M surfactant solution under load. Thick coated hairs, where the topographical fine structure component was removed, resulting in a smooth cylinder (Fig. S2 *C*), penetrated the surfactant solution at a much lower concentration of 0.001 M.

Moreover, the spring constants of the coated hairs did not alter enough to account for hair penetration (0.07 ± 0.03 Nm^{-1}, 0.06 ± 0.05 Nm^{-1}, and 0.09 ± 0.02 Nm^{-1} for the uncoated, thinly, and thickly coated hair, respectively, measured ~10 μm from the hair tip). This clearly demonstrates that the micro/nano roughness consisting of the open architecture of ridges with troughs is responsible for this effect as the chemistry is maintained (for thin and thick coats) and only the topographical component is altered. The higher adhesion values measured of thick coated hairs in comparison to thinly coated samples and uncoated samples (>1 μN, 60 ± 19 nN, and 42 ± 9 nN, respectively) also supports the previous conclusion that the channel structure is the important feature in minimizing contact with the water body.

The *Micromus tasmaniae* wing surface is composed of cells bounded by veins, from which the larger macrotrichia protrude at an angle of between 35° and 65° (Fig. 1 *C*). Small micron-sized droplets with a diameter less than vein macrotrichia spacing can come into contact with the underlying layers (microtrichia) of the wing membrane. For the latter, droplets with a diameter less than d_w (distance between hair fiber tips) can fit between the macrotrichia,

$$d_w = s_l - 2(l\cos\phi), \tag{3}$$

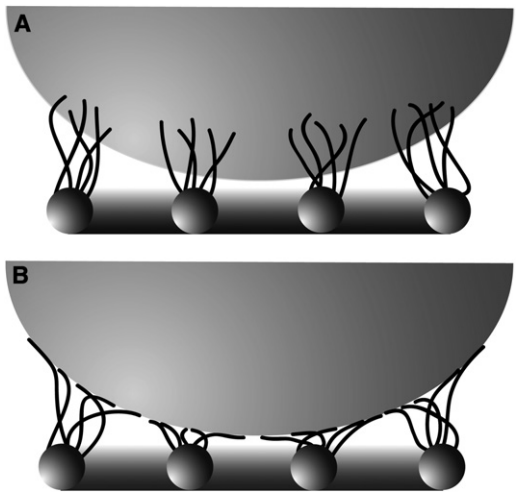

FIGURE 4 Models for droplet levitation. (*A*) Vein macrotrichia bundle together at the water/air interface. (*B*) Elastic elements hold droplet above the surface.

where l is the hair length, s_l is the distance between veins, and ϕ is the angle of hair with respect to the wing membrane as illustrated in Fig. 5.

Fig. 3, *A* and *B*, shows top and side view photographs, respectively, demonstrating that the smaller micron-sized droplets are efficiently repelled from the underlying cuticle surface in a similar fashion as larger droplets on the macrotrichia. The fine structure of the smaller hairs may also facilitate the antiwetting nature of the arrays. Indeed the scaling differences for the two different-sized hairs and the size of water droplets are not too dissimilar.

Four other lacewing species were investigated to compare their fine structure on the wings with the brown lacewing. Interestingly, none of the four species possessed microtrichia (e.g., *Italochrysa insignis* (Fig. 6 *A* and Fig. S4 *A*)), *Glenoleon pulchellus* (Fig. 6 *B* and Fig. S4 *D*), *Chrysopa oculata* (Fig. S4 *B*) and *Oligochrysa lutea* (Fig. S4 *C*)).

This beckons the question: How do these insects contend with smaller droplet sizes?

High-resolution SEM images show that the underlying membrane of these lacewings comprises a three-dimensional undergrowth of surface matting on the cuticle (Fig. 6 *B* and Fig. S4). Contact angles of small droplets on these surfaces showed that the structuring provided superhydrophobic properties (contact angles larger than 150°). Examination of the cuticle surface beneath the brown lacewing microtrichia (Fig. S1 *C*) shows that the surface is devoid of this structuring and almost completely smooth. This supports the premise that the smaller hairs are used to contend with smaller droplet sizes. Thus, the different insects (brown lacewing in relation to other lacewing species) have adopted different routes to achieving antiwetting with smaller water droplets.

Masters and Eisner (6) have shown that it is possible for green lacewings to escape from spider web entrapment partially due to the coverage of hairs on the wing membrane. In essence the authors found that the strands slide across and pull away from the hair contacts. Our results (reduced contact area and adhesion) with the brown lacewing suggest that the fine structure of the hairs may partially explain the mechanism of release and escape from spider webs. The hairs provide a similar function in this respect to that of the scales on butterflies. Fig. 7 shows diagrammatically the antiwetting hair arrangement on the brown lacewing wing. The microtrichia beneath the larger macrotrichia canopy provide additional cushioning and antiwetting behavior with larger droplets.

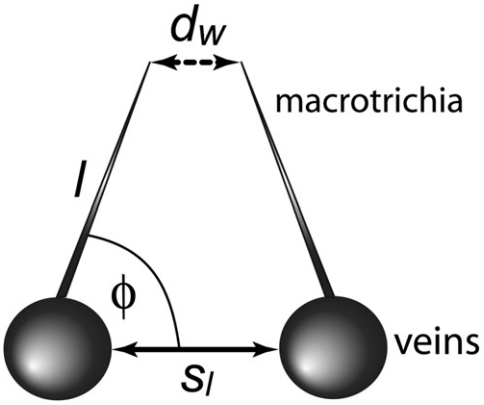

FIGURE 5 Sketch defining parameters for the expression describing the distance between hair fibers.

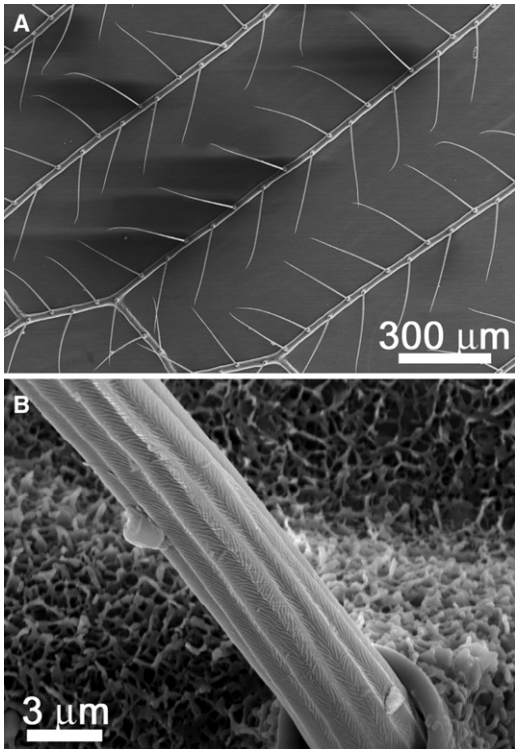

FIGURE 6 SEM images revealing a lack of fine hair structures (microtrichia) on the wings of two other lacewing species, (*A*) *Italachrga insighis* and (*B*) *Glenoleon pulchellus*.

CONCLUSIONS

The dual layer hair arrays with their specialized topographies are designed for minimizing the solid-liquid contact area and maximizing the liquid-air contact. This feature of

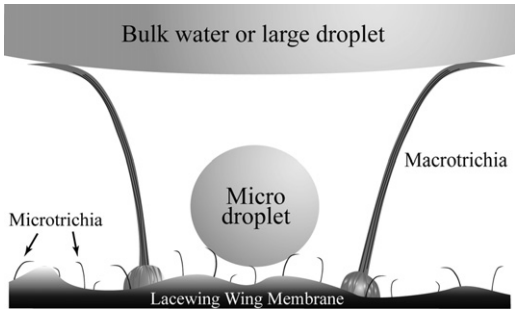

FIGURE 7 Diagrammatic representation of the antiwetting, dual hair arrangement on the lacewing wing.

multiscale defense architecture appears to be a common theme for such insects. The hair arrays demonstrate an elegant hierarchical-designed approach for minimizing interaction with water bodies of various length scales. As well, the open membrane hierarchy demonstrates a design for achieving this state utilizing minimal structural material and thus reduced weight for the insect. Weight reduction may aid the insect in terms of flight efficiency.

The special wetting properties of the brown lacewing allow the insect to interact with a variety of environmental surfaces and conditions which may constitute a hazard. For example, ponds, lakes, wetted solid surfaces (e.g., leaves), and rain all constitute conditions where an insect with high SA/M values can potentially be immobilized. Our results also support earlier hypotheses that suggested structures at this length-scale (micro/nanogrooves) found on other insects (e.g., water striders) could enhance water repellency (22,24).

SUPPORTING MATERIAL

Four figures are available at http://www.biophysj.org/biophysj/supplemental/S0006-3495(11)00039-7.

We thank S. Myhra for discussions and suggestions.

REFERENCES

1. Holdgate, M. W. 1955. The wetting of insect cuticles by water. *J. Exp. Biol.* 32:591–617.
2. Cong, Q., G.-H. Chen, …, L.-Q. Ren. 2004. Study on the superhydrophobic characteristic of butterfly wing surface. *J. Bionics Eng.* 1:249–255.
3. Wagner, P., C. Neinhuis, and W. Barthlott. 1996. Wettability and contaminability of insect wings as a function of their surface sculptures. *Acta Zoologica.* 77:213–225.
4. Vukusic, P., and J. R. Sambles. 2003. Photonic structures in biology. *Nature.* 424:852–855.
5. Gorb, S. 2001. Attachment Devices of Insect Cuticle. Kluwer Academic, New York, 21–36.
6. Masters, W. M., and T. Eisner. 1990. The escape strategy of green lacewings from orb webs. *J. Insect Behav.* 3:143–157.
7. Watson, G. S., S. Hu, …, J. A. Watson. 2010. Micro and nanostructures found on insect wings—designs for minimizing adhesion and friction. *Int. J. Nanomanufactur.* 5:112–128.
8. Gorb, S. N., A. Kesel, and J. Berger. 2000. Microsculpture of the wing surface in Odonata: evidence for cuticular wax covering. *Arthropod Struct. Dev.* 29:129–135.
9. Watson, G. S., S. Myhra, …, J. A. Watson. 2008. Putative functions and functional efficiency of ordered cuticular nanoarrays on insect wings. *Biophys. J.* 94:3352–3360.
10. Sun, M., G. S. Watson, …, A. Liang. 2009. Wetting properties on nanostructured surfaces of cicada wings. *J. Exp. Biol.* 212:3148–3155.
11. Cassie, A. B. D., and S. Baxter. 1944. Wettability of porous surfaces. *Trans. Faraday Soc.* 49:546–551.
12. Gao, L., and T. J. McCarthy. 2007. How Wenzel and Cassie were wrong. *Langmuir.* 23:3762–3765.
13. Wenzel, R. N. 1936. Resistance of solid surfaces to wetting by water. *Ind. Eng. Chem.* 28:988–994.
14. Herminghaus, S. 2000. Roughness-induced non-wetting. *Europhys. Lett.* 52:165–170.
15. Shirtcliffe, N. J., G. McHale, …, M. I. Newton. 2010. An introduction to superhydrophobicity. *Adv. Colloid Interface Sci.* 161:124–138.
16. Watson, G. S., J. A. Blach, …, S. Myhra. 2004. Interactions of poly (amino acids) in aqueous solution with charged model surfaces—analysis by colloidal probe. *Biosens. Bioelectron.* 19:1355–1362.
17. Cleveland, J. P., S. Manne, …, P. K. Hansma. 1993. A non-destructive method for determining the spring constant of cantilevers for scanning force microscopy. *Rev. Sci. Instrum.* 64:403–405.
18. Watson, G. S., B. P. Dinte, …, S. Myhra. 2002. Demonstration of atomic scale stick-slip events stimulated by the force versus distance mode using atomic force microscopy. *J. Phys. D Appl. Phys.* 35:2066–2074.
19. Blach-Watson, J. A., G. S. Watson, …, S. Myhra. 2004. UV patterning of polyimide: differentiation and characterization of surface chemistry and structure. *Appl. Surf. Sci.* 235:164–169.
20. Boreyko, J. B., and C.-H. Chen. 2009. Self-propelled dropwise condensate on superhydrophobic surfaces. *Phys. Rev. Lett.* 103:184501.
21. Otten, A., and S. Herminghaus. 2004. How plants keep dry: a physicist's point of view. *Langmuir.* 20:2405–2408.
22. Gao, X., and L. Jiang. 2004. Biophysics: water-repellent legs of water striders. *Nature.* 432:36.
23. Sun, M., C. Luo, …, Y. Chen. 2005. Artificial lotus leaf by nanocasting. *Langmuir.* 21:8978–8981.
24. Watson, G. S., B. W. Cribb, and J. A. Watson. 2010. How micro/nanoarchitecture facilitates anti-wetting: an elegant hierarchical design on the termite wing. *ACS Nano.* 4:129–136.